Drug Design, Development and Therapy

Dovepress

open access to scientific and medical research

Open Access Full Text Article

ORIGINAL RESEARCH

Beneficial Effects of Echinacoside on Diabetic Cardiomyopathy in Diabetic *Db/Db* Mice

This article was published in the following Dove Press journal:
Drug Design, Development and Therapy

Xiang Zhang
Yarong Hao

Department of Geriatrics, Renmin Hospital of Wuhan University, Hubei, People's Republic of China

Purpose: In this study, we investigated the protective effects and mechanism of action of echinacoside (ECH) from cistanche tubulosa extract in cardiomyocytes of *db/db* diabetic mice.

Methods: Twenty healthy male *db/db* mice aged 8 weeks were randomly divided into *db/db* +ECH (n=10, ECH, 300 mg/(kg/d)), *db/db* (n=10, saline), and *db/m* control groups (n=9). Mice were monitored weekly for diet and activity. Mice were injected with 2% of pentobarbital sodium in week 10 and executed. Weight and free blood glucose (FBG) were measured weekly. Echocardiographs were used to detect cardiac function. HE staining, Sudan II staining, Masson's trichrome staining and Tunel assays were used to evaluate myocardial tissue pathological changes, collagen fiber deposition, lipid accumulation and apoptosis rates in cardiomyocytes, respectively. Western blot and RT-PCR analysis were used to detect the expression of components of the PPAR-α/M-CPT-1 and p53/p38MAPK signaling axis.

Results: Compared to *db/db* mice, ECH groups showed lower blood glucose and lipid levels. Deterioration in cardiac function was also delayed following ECH treatment. Histopathological analysis showed that ECH significantly improved myocardial tissue in *db/db* mice, including reduced intercellular spaces, regular arrangements, improved extracellular matrix deposition, and reduced lipid accumulation. ECH also significantly reduced oxidative stress levels in myocardial tissue in *db/db* mice. Moreover, ECH inhibited PPAR-α/M-CPT-1 signaling, downregulated CD36, and upregulated glucose transporter type 4 (GLUT-4) expression in *db/db* mouse models of DCM. ECH also inhibited p53/p38MAPK signaling, downregulated caspase-3 and caspase-8, and upregulated Bcl-2/Bax in *db/db* mouse models of DCM.

Conclusion: ECH displays protective effects in DCM, including the inhibition of cardiac apoptosis and oxidative stress, and improved lipid metabolism in cardiomyocytes. ECH also inhibits cardiac apoptosis through its regulation of p53/p38MAPK signaling, and prevents lipid accumulation through suppression of the PPAR-α/M-CPT-1 signaling axis.

Keywords: diabetic cardiomyopathy, echinacoside, lipid metabolism disorders, PPAR-α, p53/p38MAPK signaling

Introduction

Diabetic cardiomyopathy (DCM) is a major complication of diabetes, with high morbidity and a high risk of cardiovascular disease and mortality in diabetic patients.[1] The incidence of DCM in patients with a history of diabetes ≥ 5 years is over 44.4%, which increases to 56% after 8 years.[2,3]

DCM is a kind of primary cardiomyopathy, which is manifested as cardiac structural and functional abnormalities caused by myocardial fibrosis cell apoptosis and microvascular lesions in diabetic patients without ischemic or hypertensive

Correspondence: Yarong Hao
Department of Geriatrics, Renmin Hospital of Wuhan University, 99 Zhang Zhidong Road, Wuchang District, Wuhan, Hubei Province, People's Republic of China
Tel +86 18827688568
Email 984022801@qq.com

submit your manuscript | www.dovepress.com
DovePress
http://doi.org/10.2147/DDDT.S276972

heart disease, and can induce cardiac arrhythmia with cardiac origin shock and sudden death in heart failure.[4] Due to the complex pathogenesis of DCM and its diagnosis at advanced stages, no effective treatments exist.[5] Hyperglycemia is the initiating factor during DCM pathogenesis. Long-term hyperglycemia results in disturbed glucose and lipid metabolism in the cardiomyocytes of diabetic patients, leading to injury to vascular endothelial cells and other tissues, promoting pathological changes including hypertrophy, necrosis, apoptosis and myocardial interstitial fibrosis.[6,7] Glucose and lipid metabolism disorders are key to the pathological mechanisms of DCM. The effective control of energy metabolism in cardiomyocytes therefore represents an important therapeutic strategy for DCM.

Myocardial lipid accumulation in DCM exacerbates the progression of heart failure. PPAR-α is a key regulator of various related genes in the fatty acid oxidation system of cell peroxidases, mitochondria and microsomes, and plays a key role during lipid metabolism and the regulation of inflammation and immunity.[8] PPAR-α improves lipid metabolism through mitochondrial and peroxidase fatty acid beta oxidation, mediated through carnitine palmitoyl transferase-I (CPT-I).[9] The oxidation of long and branched fatty acids[10] reduces the synthesis and assembly of lipoproteins and VLDL.[11] The indirect regulation of bile acid synthesis promotes cholesterol excretion[12] and inhibits the expression of inflammatory-associated genes. PPAR-α expression in the liver is significantly lower in patients with non-alcoholic fatty liver disease or in animal models of long-term high-fat consumption.[13,14] Everett et al showed that the levels of liver associated free fatty acids significantly increased in *PPAR-α knockout* mouse models due to attenuated lipid metabolism, promoting liver steatosis.[15] These findings suggest that PPAR-α plays an important role in the pathogenesis of lipid metabolism.

Echinoside (ECH) is a natural compound isolated from the stems of cistanche tubulosa. The active chemical of ECH is phenylethanoside, which displays antioxidant, anti-fatigue, anti-tumor and anti-inflammatory effects, and can improve memory, nerve and liver protection, and enhance immune regulation.[16,17] In the study on *db/db* diabetic mice, it was found that ECH could improve insulin resistance, increase HDL level, and reduce TG, TC and LDL levels, indicating that ECH could effectively improve diabetic lipid metabolism.[18] In addition, Shimoda et al proved that echinoside could affect lipid metabolism by regulating mRNA related to hepatobiliary sterol transport and metabolism.[19] Previous studies have shown that ECH regulates the expression of TGF-β and its downstream genes to improve renal fibrosis in *db/db* mice.[20] In this study, to further understand the protective effects of ECH on myocardial cell injury in DCM and to explore its potential molecular mechanisms, we used *db/db* mice as a DCM disease model, and explored the regulatory mechanism(s) of ECH on proteins that control glucose and lipid metabolism disorders, oxidative stress, and apoptosis in cardiomyocytes. Our aim was to provide a theoretical basis for the effective treatment of DCM.

Materials and Methods

Chemicals and Reagents

ECH powder (94% purity detected by HPLC, Batch No.190906) (Supplement Figure 1) was obtained from Shanghai Medical Science Company, Ltd. (Shanghai, China). ECH was dissolved in water to 2 mg/mL and stored at 4°C in the dark. ECH was administered at a dose of 100–500 mg/kg·d and significantly lowered blood glucose and improved blood lipid levels.[18] ECH displayed dose-dependent hypoglycemic and anti-hyperlipidemic effects.

Experimental Animals and Treatment

Animal experiments were performed in accordance with the National Institutes of Health guidelines (NIH Pub. No 85-23, revised 1996). Protocols were approved by the experimental animal ethics committee and Animal Feeding Center of Renmin Hospital of Wuhan University (Wuhan, China, No. 20190517). Adult male *C57BLKS/J db/db* mice and *db/m* mice (SPF grade) were purchased from Nanjing University–Nanjing Biomedical Research Institute (Nanjing, People's Republic of China, number: SCXK (Sue) 2018-0001). Animals were caged in the Animal Center of Renmin Hospital (Wuhan, People's Republic of China) at room temperature (20°C), relative humidity of 50%-60%, and subject to a 12-h light/dark cycle. Adaptive feeding was performed for 1 h and no hypoglycemic drugs were administered.

Following quarantine, *db/db* mice were randomly assigned to the diabetes model group (*db/db* group, n= 10), ECH treatment group (*db/db*+ECH group, n=11) or *db/m* control group (db/m, n=9). At 8 weeks, mice in the *db/db* and *db/m* groups were administered oral 0.05 mL/10g body weight saline for 10 weeks, whilst mice in the *db/db*+ECH group were administered 300 mg/(kg/d) oral

ECH according to body weight for 10 weeks. The body weights of the three groups of mice were monitored weekly, and feeding, drinking and activity were assessed. Once mice had fasted for 8 h, blood samples (~50ul) were taken from the end of the tail every 2 weeks with a blood glucose meter and test paper (Johnson & Johnson, New Brunswick, NJ, USA) to determine blood glucose levels. After 10 weeks of intervention, mice were anesthetized by intraperitoneal injection with 2% pentobarbital sodium (Shanghai Harvest company, Shanghai, People's Republic of China) (100mg/kg). Blood was collected following capillary needle insertion and serum was rapidly separated and stored at −80°C for analysis. Following cardiac perfusion with cold- PBS to remove the blood, free PBS was removed with filter paper. Cardiac tissue was separated and weighed, and the dry weight of the heart was measured. The abdomen of mice was shaved, the abdomen was opened after alcohol (70%) disinfection, and the subcutaneous adipose tissue of the abdomen was quickly removed and the weighed wet. The tibia of the mice were isolated and measured. Cardiac hypertrophy was assessed through the ratio of heart weight to tibial length (HW/TL) (mg/mm). Cardiac tissues were fixed with 4% paraformaldehyde (Google biotechnology, Wuhan, People's Republic of China) and biopsies were performed to monitor the morphology of myocardial tissue. The remaining cardiac tissue was placed in liquid nitrogen for 1 h and stored at −80°C prior to RT-PCR and Western blot analysis.

Echocardiography

Ultrasound (VisualSonics, Toronto, ON, Canada) was performed for echocardiographic measurements at the end of the experiment. Mice were anesthetized by intraperitoneal injection of 4% chloral hydrate at 30mg/kg for half an hour,[21] shaved to expose the chest area, and fixed onto a flat plate. The left ventricular systolic diameter (LVDs), LV diastolic diameter (LVDd), LV ejection fraction (EF), and LV fractional shortening (FS) were determined.

Metabolic and Biochemical Parameters

At 18 weeks of age, blood samples were centrifuged at 4°C for 20 min for serum collection. A total automated biochemical analyzer (ADVID2400, Tokyo, Japan) was used to detect total cholesterol (TC), triglycerides (TG), free fatty acids (FFAs), high-density lipoprotein-cholesterol (HDL-c), and low-density lipoprotein-cholesterol (LDL-c) in the serum.

Oxidation Index and Antioxidant Levels

Fresh left ventricular myocardial tissues (50 mg) of each group were obtained. The levels of SOD, GSH-px and MDA in the myocardial cells were determined using commercial kits (Nanjing Jiangcheng Bioengineering Institute, China).

Cardiac Histology, HE, Masson's Trichrome, Tunel and Sudan II Staining

The left ventricular region of the myocardial tissue of each group of mice were fixed in 4% paraformaldehyde for 24h, paraffin embedded, sectioned and HE stained. Pathological and morphological changes of the myocardial fibers of each group of mice were observed under light microscopy (JEOL, Tokyo, Japan). Cardiac myocyte apoptosis was detected by Tunel assays (number11684817910, Roche, USA). Heart tissue was pre-treated with paraformaldehyde, embedded and sliced. Sections were washed with xylene I (Shanghai, People's Republic of China) (20 min) -xylene II (20 min) -anhydrous ethanol I (10 min) -anhydrous ethanol II (10 min) −95% alcohol (5 min)-90% alcohol (5 min)-80% alcohol (5 min) −70% alcohol (5 min) and distilled water. Sections were dried through shaking and histochemical brush rings were used to prevent liquid loss. Protease K was added to the rings to cover the tissue. Following incubation at 37°C for 15 min, slides were placed in PBS (pH 7.4) and washed in a decolorizing shaker (three times for 5 min). Reagents 1 (TdT) and 2 (dUTP) were mixed at a ratio of 1:9 and added to the inner covering of the tissue. Mixtures were incubated in a water bath at 37°C for 60 min. A small volume of water was added to maintain humidity. Slides were rinsed in PBS and DAPI stained (Aspen biological, Wuhan, People's Republic of China) in the dark for 5 min. Slides were rinsed in PBS and mounted using anti-fluorescence quenching agent. Sections were visualized by fluorescent microscopy and imaged. Sudan II staining was used to observe lipid accumulation in the cardiac myocytes. Left ventricular tissues were fixed in 10% paraformaldehyde for 30 min, stained with Sudan red II (Gefan, Shanghai, People's Republic of China) at room temperature for 10 min, decolorized with 75% alcohol, and re-stained in PBS for 15 min. The ratio of the myocardial fibrosis to total area in Masson's stained trichrome sections was determined using Image-Pro Plus quantitative software. Slides were mounted using glycerine gelatin and imaged via microscopy.

Western Blot Analysis

Heart tissues (~50 mg) were sectioned using tissue scissors and lysed. Phenylmethylsulfonyl fluoride (PMSF) was added to prevent protein degradation (1 mmol/L). Samples were centrifuged at 1200 rpm for 10 min. Protein concentrations were determined by BCA assay. Proteins were denatured in an equal volume of SDS-PAGE loading buffer (2X) and boiled for 10 min. Samples (~50 ug) were resolved by SDS-PAGE electrophoresis, and wet transferred to PVDF membranes. Membranes were blocked in 5% non-fat milk (Erie Inc., Hubei, Peoples Republic of China) for 1 h and probed overnight at 4°C with primary antibodies against PPAR-α (1:1000 dilution; CST, Danvers, MA, USA), M-CPT-1 (1:1000 dilution; CST), CD36 (1:1000 dilution; CST), GLUT-4 (1:1000 dilution; CST), p53 (1:1000 dilution; Abcam), p38-MAPK (1:1000 dilution; Abcam), caspase-3 (1:1000 dilution; Abcam, Cambridge, MA, USA) and caspase-8 (1:1000 dilution; Abcam). Membranes were labeled with the indicated secondary antibodies at room temperature for 1 h and developed. Gray values of each protein band were analyzed.

RT-PCR Analysis

Total RNA was extracted from the heart tissues of mice in each group (100 mg) using Trizol (Thermo Fisher Scientific, Waltham, MA, USA). RNA purity and concentrations were detected by UV spectrophotometry. RNA integrity was confirmed by electrophoresis. Reverse transcription was performed using commercial RT kits (Takara, Tokyo, Japan). Samples were denatured at 95°C for 30s, followed by 40 cycles of: 95°C for 5s; 60°C for 40s; 95 °C for 15 s; 60 s at 60 °C, 95 °C for 15 s. MRNA levels were assessed using the SYBR Green RT quantitative reverse transcription-PCR (ABI 7500; Thermo Fisher Scientific) using the 2-ΔΔCt method. GAPDH mRNA levels were assessed as an internal control. Primer sequences are shown in Table 1.

Statistical Analyses

SPSS22.0 (IBM Corporation, Armonk, NY, USA) software was used for statistical analysis. Measurement data were expressed as the mean ± standard deviation (x±s). A one-way ANOVA was performed for group comparisons. Univariate analysis was used to evaluate differences amongst the groups. Groups were compared using the minimum significant difference method (LSD) to obtain uniform data. Non-normal distribution data were analyzed using Dunnett's tests. P-values≤0.05 indicated significant differences.

Results

Effects of ECH on Db/Db Mice

Mice in the *db/db* groups showed obvious polyphagia and polyuria. Body sizes were also significantly larger than those of the *db/m* mice. Body weights in the *db/db* group significantly increased relative to the *db/m* group (Figure 1A; $^{**}p<0.01$). Body weights of the *db/db* + ECH group were significantly lower than those of the *db/db* group after 10 weeks of ECH treatment (Figure 1A; $^{\#}p<0.05$). At week 15, the difference in body weight of each group gradually appeared after ECH intervention. Abdominal fat thickness of mice in the *db/db* group was higher than those of the *db/m* group (Figure 2B; $^{*}p<0.01$). ECH, therefore, improves obesity in *db/db* mice, the specific mechanisms of which require further assessment.

Fasting blood glucose levels were assessed on a weekly basis. As shown in Figure 1B, compared to *db/m* mice, fasting blood glucose levels of the *db/db* mice significantly increased with age and showed obvious hyperglycemia (Figure 1B; $^{*}p<0.01$). Over a 10 week period, fasting

Table 1 RT Fluorescence Quantitative PCR Primers

Genes	Forward Primer 5′-3′	Reverse Primer 5′-3′	Fragment Length (bp)
GAPDH	CCTCGTCCCGTAGACAAAATG	TGAGGTCAATGAAGGGGTCGT	133
PPAR-α	CTCGGAGGGCTCTGTCATCA	TGCGTGGACTCCATAGTGGT	319
M-CPT-1	CCCATGTGCTGCCTACCAGAT	CCTTGAAGAAGCGACCTTTG	218
GLUT-4	GCTTCTGTTGCCCTTCTGTC	TGGACGCTCTCTTTCCAACT	166
CD36	TCTTCCAGCCAACGCCTTT	CCTTCTTTGCACTTGCCATGTCC	126
P53	TATGGCTTCCACCTGGGCTT	TCTTCCAGATACTCGGGATACAA	306
P38MAPK	TGCCCGAACGTACCAGAAC	CCTTTTGGCGTGAATGATGGA	142
Caspase-3	GTCTGACTGGAAAGCCGAAAC	GACTGGATGAACCACGACCC	205
Bcl-2	GCTACCGTCGTGACTTCCCA	CATCCCAGCCTCCGTTATCC	270
Bcl-x	CGTGGAAAGCGTAGACAAGGA	TGCTGCATTGTTCCCGTAGAG	148

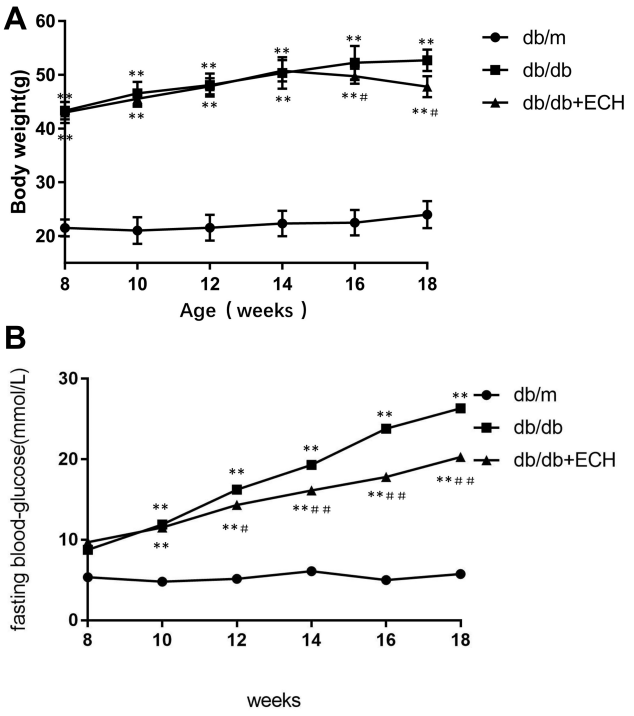

Figure 1 Effects of ECH on body weight (**A**) and fasting blood glucose levels (**B**) of *db/db* mice.
Notes: Data are expressed as mean±SD. db/m group n=9, n=10 for all other groups; **p < 0.01 vs db/m group, #p < 0.05 or ##p<0.01 vs db/db group.
Abbreviation: ECH, echinacoside.

blood glucose levels in the *db/db* and *db/db* + ECH group increased, whilst glucose levels in the *db/m* group remained stable. Fasting blood glucose levels in the *db/db* + ECH group were slower than those of the *db/db* group (Figure 1B; ##p<0.01), suggesting that ECH markedly improved hyperglycemia in *db/db* diabetic mice. We speculated that ECH could promote the synthesis of liver glycogen and inhibited activity of α-glucosidase to suppressed glucose transport in the small intestine, significantly contributing to hypoglycemia.[22,23]

Effects of ECH on the Biochemical Parameters of Db/Db Mice

Three mice from each group were assessed via HW/TL analysis. HW/TL in the *db/db* group significantly increased relative to the *db/m* group [Figure 2A; (8.05 ±0.92) vs (6.48±0.67).*p<0.05]. The HW/TL of the *db/db* + ECH group was significantly lower than the *db/db* group [Figure 2A; (6.98±0.05) vs (8.05±0.92). #p<0.05] after 10 weeks of treatment. These results suggested that cardiac hypertrophy occurred in *db/db* mice, which significantly improved after 10 weeks of ECH intervention.

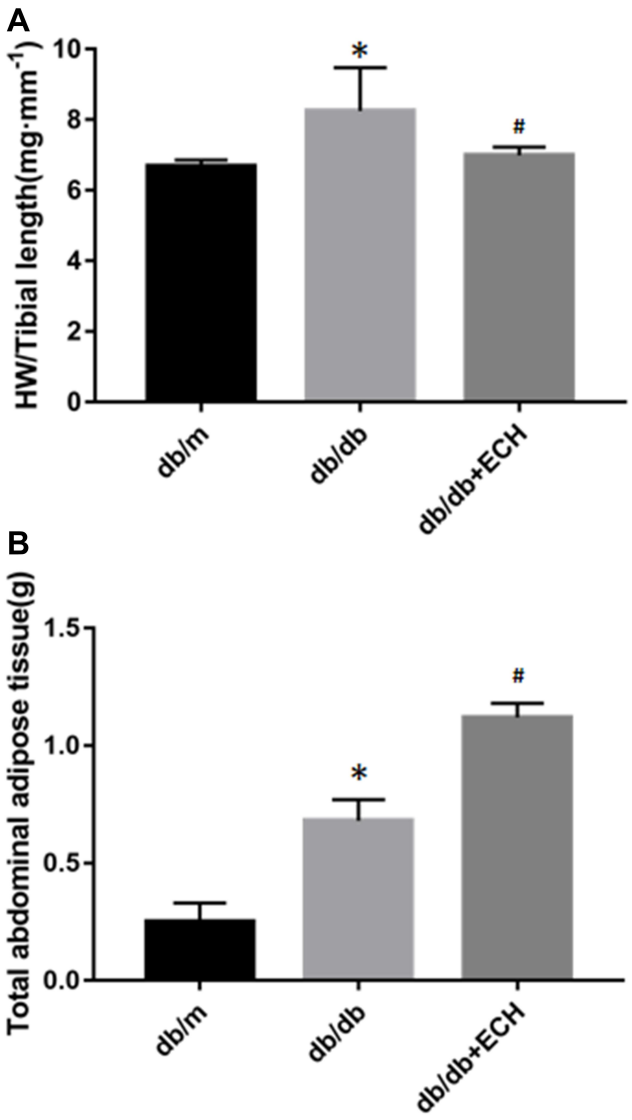

Figure 2 Effects of ECH on HW/TL of *db/db* mice (**A**) and abdominal fat thickness of mice (**B**) of *db/db* mice.
Notes: Data are expressed as mean±SD. db/m group n=9, all other groups n=10; *p < 0.05 vs db/m group, #p < 0.05 vs db/db group.
Abbreviations: ECH, echinacoside; HW, heart weight; TL, tibial length.

At the end of the 18 week period, blood serum TC, TG, FFA and LDL-c significantly declined in the *db/db* + ECH group relative to the *db/db* group. HDL-c levels significantly increased (Table 2; ##P<0.01). These results suggest that ECH has protective effects on cardiac function and lipid metabolism in *db/db* mice, which could partly explain the weight loss observed in *db/db* mice.

ECH Alleviates Cardiac Dysfunction in Db/Db Mice

Echocardiographic data showed that the ejection fraction (EF%) and fractional shortening (EF%) were

Table 2 Effect of ECH on Serum Lipid Metabolism Levels in Db/Db Mice

Groups	TC(mmol/L)	TG(mmol/L)	FFA(mmol/L)	HDL-c(mmol/L)	LDL-c(mmol/L)
db/m (n=9)	2.08±0.36	0.97±0.15	0.28±0.12	1.11±0.21	0.15±0.37
db/db (n=10)	3.57±1.07**	1.93±0.71**	3.66±0.07**	1.00±0.13**	1.40±0.15**
db/db+ECH (n=10)	3.13±0.66##	1.53±0.66##	1.41±0.04##	1.40±0.31##	0.21±0.13##

Notes: Data are presented as mean ± SD. **P<0.01 compared with the db/m group;##P<0.01 compared with the db/db group.
Abbreviations: TC, total cholesterol; TG, triglyceride; FFA, free fatty acid; HDL-c, high-density lipoprotein-cholesterol; LDL-c, low-density lipoprotein-cholesterol; ECH, echinacoside.

significantly lower in *db/db* mice (36.14%±3.40% and 37.21%±3.42%) compared to non-diabetic mice (*db/m*) (72.26%±3.29% and 46.69%±2.69%). Similarly, the left ventricular eject fraction (LVEF%) was markedly smaller in *db/db* mice (61.52%±0.55%) compared to *db/m* (70.36%±3.61%) mice. Left ventricular end-systolic dimensions (LVDs) and left ventricular end-diastolic dimensions (LVDd) were significantly higher in *db/db* mice (2.82mm±0.18mm and 4.19mm±0.37mm) compared to non-diabetic controls (*db/m*), (2.51mm ±0.23mm and 3.98mm ±0.33mm), suggesting that cardiac function was impaired by diabetes. Notably, in *db/db* mice administered ECH EF%, FS% and LVEF% were effectively restored to 63.24%±3.36%, 2.18% ±3.38% and 64.98%±2.11%, respectively (Figure 3A, B, E and F). In addition, after 10 weeks of ECH intervention, LVDs and LVDd were significantly reduced to 2.68 mm±0.26mm and 4.02mm ±0.27 mm, respectively (Figure 3C and D).

Effects of ECH on Cardiac Morphology in Db/Db Mice

Heart tissues were collected for HE staining, Masson's trichrome staining and Sudan II staining. Structural changes were assessed by microscopy (Figures 4 and 5). HE staining showed that the hearts of the *db/m* group were normal, with clear and compact arrangements of cardiac cells, and clear structures. However, obvious hypertrophy and necrosis were evident in the myocardial cells of the *db/db* group. Compared to the *db/db* group, the morphology of myocardial cells in *db/db*+ECH group recovered, intercellular spaces were reduced, and the arrangements were regular. Masson staining revealed collagen fiber deposition in the heart tissues of *db/db* mice (Figure 5). After the 10-weeks of ECH treatment, fibrosis and

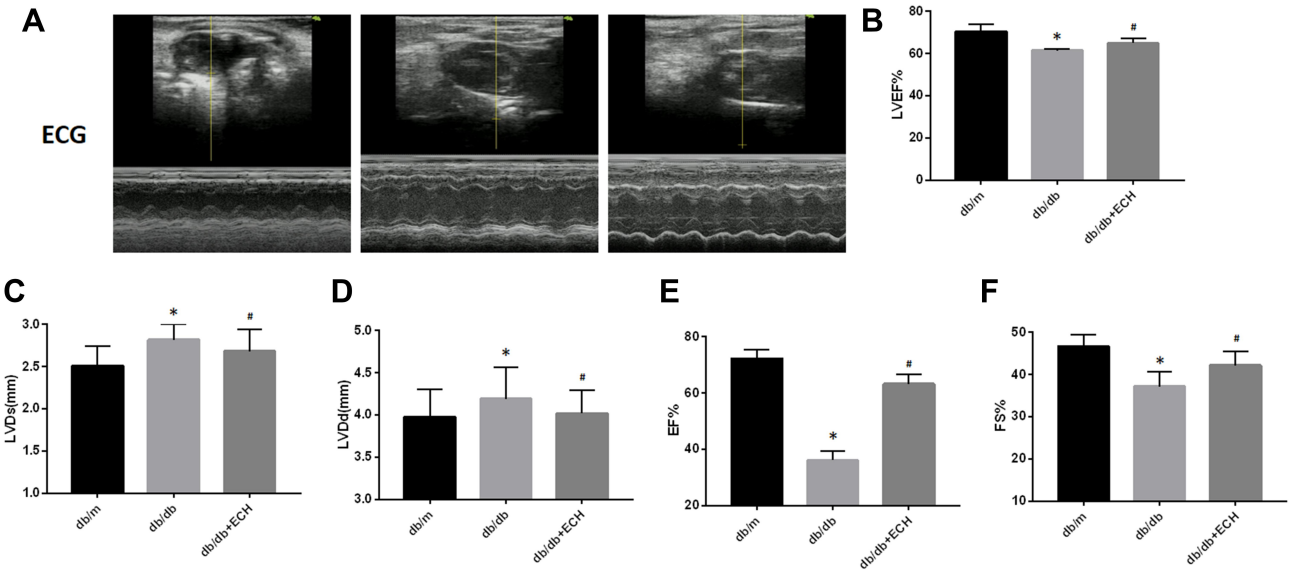

Figure 3 Effects of echinacoside (ECH) on impaired cardiac function of *db/db* mice. (**A**) Echocardiography (ECG) of *db/db* mice. (**B**) ECH increases the DM-induced reduction of LVEF. (**C**) ECH rescues the DM-induced increase of LVDs. (**D**) ECH rescues the DM-induced increased of LVDd. (**E**) ECH increases the DM-induced reduction of EF. (**F**) ECH increases the DM-induced reduction of FS.
Notes: Data are expressed as mean±SD. db/m group n=9, the other groups n=10; *p < 0.05 vs db/m group, #p < 0.05 vs db/db group.
Abbreviations: ECH, echinacoside; DM, diabetes mellitus; LVEF, left ventricular eject fraction; LVDs, left ventricular end-systolic dimension; LVDd, left ventricular end-diastolic dimension.

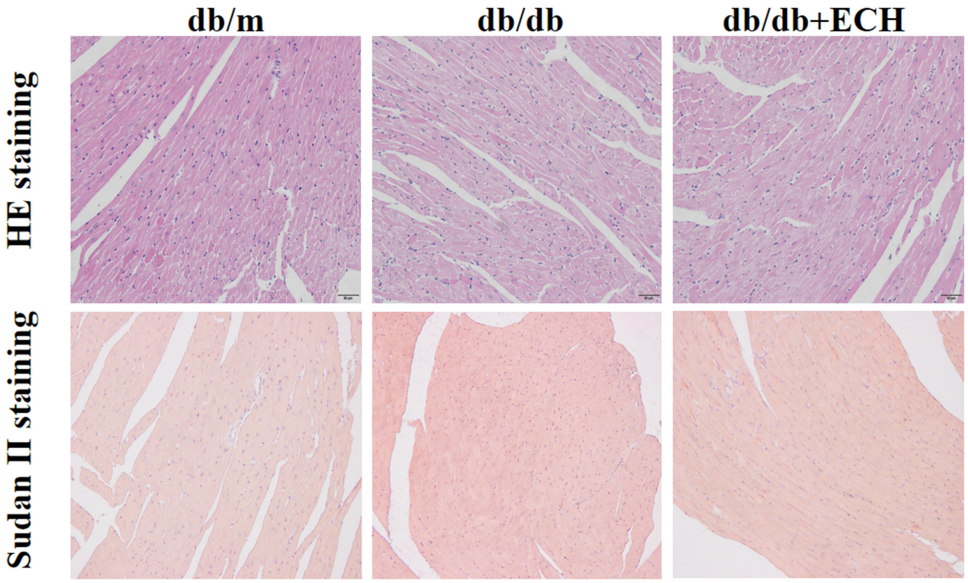

Figure 4 Effects of ECH on morphologic changes in the hearts of *db/db* mice (200×).

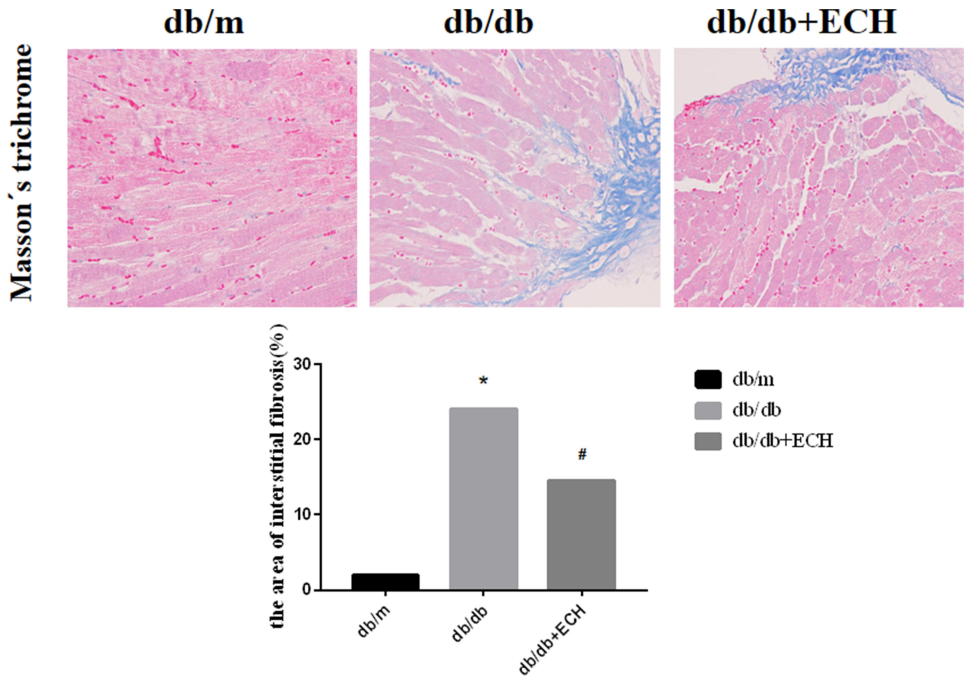

Figure 5 Effects of ECH on interstitial fibrosis in the heart of *db/db* mice (400x).
Notes: Data are expressed as mean±SD. db/m group n=9, all other groups n=10; *p < 0.01 vs db/m group, #p < 0.01 vs db/db group.
Abbreviation: ECH, echinacoside.

collagen development in *db/db* mice were significantly inhibited. According to statistical assessments of fibrosis levels (Figure 5), the area of interstitial fibrosis in *db/db* mice was significantly larger than *db/m* mice, although ECH treatment significantly reduced the fibrosis area ($p<0.05$). Sudan II staining showed that myocardial cells in *db/m* group had few lipid droplets and low levels of lipid degeneration. Severe lipid degeneration was observed in the myocardial cells of the *db/db* group, and lipid vacuoles of different sizes were observed. Lipid deposition in the myocardial cells of mice significantly declined after ECH treatment, confirming its therapeutic effects.

Effects of ECH on Cardiomyocyte Injury in Db/Db Mice

Myocardial injury in DCM occurs as a result of oxidative stress-induced apoptosis. Tunel staining was used to detect apoptosis rates in each group. Compared to the *db/m* group, the total apoptosis rates of cardiomyocytes in the *db/db* group significantly increased [Figure 6; (31.66 ± 2.89%) vs (1.86 ± 0.49%). **p < 0.01]. Compared to the *db/db* group, the apoptosis rates of mice in the *db/db*+ECH group significantly decreased [Figure 6; (8.35 ± 1.13%) vs (31.66 ± 2.89%). $^{\#\#}$p < 0.01], indicating that ECH significantly alleviated apoptosis rates in the *db/db* cardiomyocytes. To explore whether the cardiomyocytes in each group were under oxidative stress, relevant oxidative and antioxidant indexes including superoxide dismutase (SOD), glutathione peroxidase (GSH-px) and malondialdehyde (MDA) were measured. As shown in Figure 7, compared to the *db/m* group, the expression of SOD and GSH-px in the *db/db* group significantly decreased, whilst the expression of MDA significantly increased (Figure 7; **p<0.01). However, after 10 weeks of ECH intervention, the above indexes of *db/db* mice were significantly improved (Figure 7; $^{\#\#}$p<0.01). ECH reduced apoptosis in the cardiomyocytes of *db/db* mice through its ability to reduce oxidative stress. After 10 weeks, ECH reduced inflammation and intracellular calcium concentrations, protecting cells from myocardial injury. These effects now require further investigation in future studies.

We further examined the expression of apoptosis associated signaling pathways in cardiomyocytes, including p53, p38MAPK, caspase-3, caspase-8 and Bcl-2/Bax. The expression of p53, p38MAPK and caspase-3 in the heart tissues of *db/db* mice was significantly higher than those of the *db/m* group (Figure 8, Supplement Table 1). Compared to the *db/db* group, p53, p38MAPK and caspase-3 levels decreased in the *db/db*+ECH group, and Bcl-2/Bax mRNA levels were significantly lower. These results suggest that the activation of p53/p38MAPK axis in diabetic mice increased caspase-3 and caspase-8 expression, and initiates apoptosis. The expression of the anti-apoptotic gene Bcl-2 was suppressed whilst the expression of the pro-apoptotic gene Bax was up-regulated, eventually leading to cardiac apoptosis (Figure 8B, Supplement Table 2). Following ECH gavage,

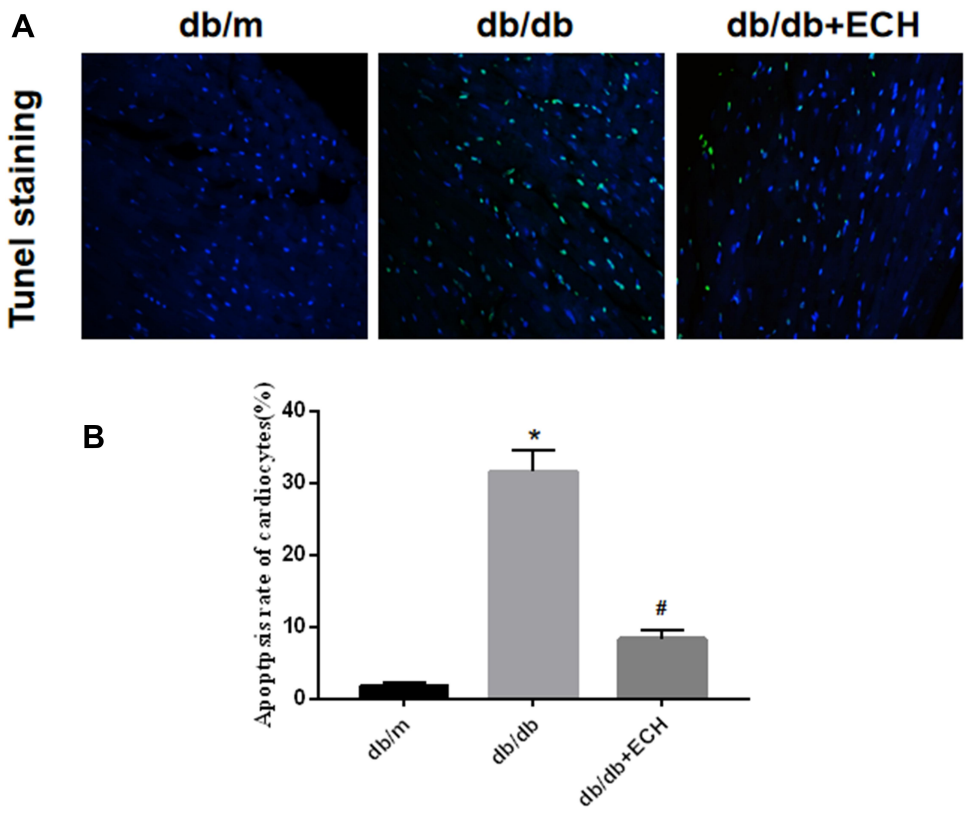

Figure 6 Tunel staining of cardiac myocytes (**A**) and apoptosis rates of cardiac myocytes (**B**). Original magnification x 400.
Notes: db/m group n=9, the other groups n=10; *p < 0.01 vs db/m group, $^{\#}$p < 0.01 vs db/db group.
Abbreviation: ECH, echinacoside.

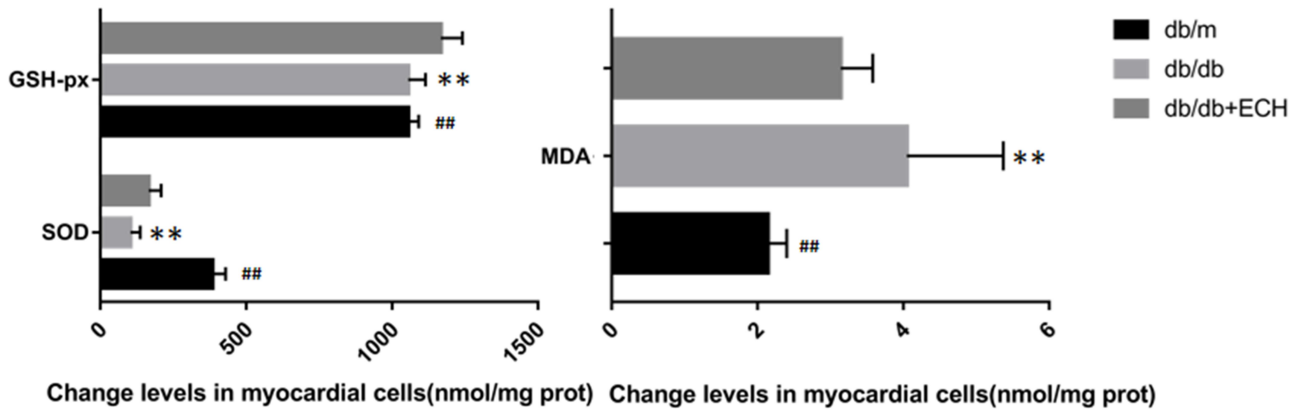

Figure 7 Effects of ECH on oxidative damage in the cardiac myocytes of *db*/*db* mice.
Notes: Data are expressed as mean±SD. db/m group n=9, all other groups n=10; **p < 0.01 vs db/m group, ##p < 0.01 vs db/db group.
Abbreviations: ECH, echinacoside; SOD, superoxide dismutase; GSH-px, glutathione peroxidase; MDA, malondialdehyde.echinacoside.

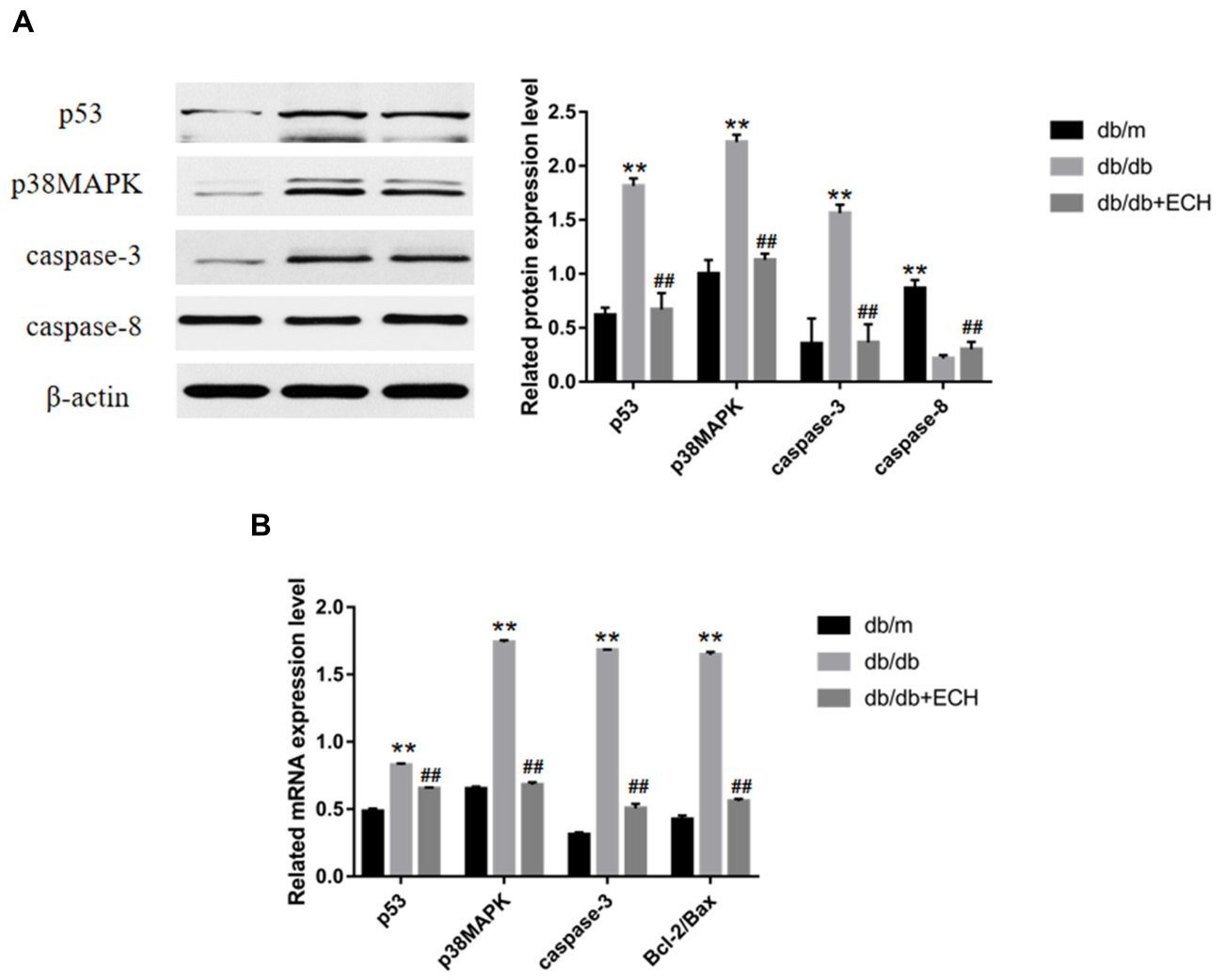

Figure 8 Western blot analysis of p53, p38MAPK, caspase-3, caspase-8 (**A**) and RT-PCR analysis of p53, p38MAPK, caspase-3, bcl-2/bax (**B**).
Notes: Data are expressed as mean±SD. db/m group n=9, the other groups n=10; **p < 0.01 vs db/m group, ##p < 0.01 vs db/db group.
Abbreviations: ECH, echinacoside; p38MAPK, p38-mitogen-activated protein kinases; caspase, cysteinyl aspartate specific proteinase.

db/db mice showed lower levels of p53/p38MAPK activity and cardiac muscle cell apoptosis. These effects were consistent with the cardiac histological changes observed following HE staining and Tunel assays, confirming the protective effects of ECH (Figures 4 and 6).

ECH Activates Cardiac PPAR-α/M-CPT-1 Signaling in Db/Db Mice

Suppression of the M-CPT-1 (muscle-carnitine palmitoyl transferase-1) pathway and its subsequent nuclear translocation leads to PPAR-α- mediated lipid metabolism associated abnormities in DCM.[24] PPAR-α, M-CPT-1 and CD36 expression were assessed by Western blot and RT-PCR analysis (Figure 9, Supplement Tables 3 and 4). The results showed that PPAR-α, M-CPT-1 and GLUT-4 mRNA levels in the *db/db* groups were lower than those of the *db/m* group (**p<0.01). CD36 expression was also higher in the *db/m* group (**p<0.01), suggesting that PPAR-α/M-CPT-1 signaling was inhibited in the *db/db* group. PPAR-α and M-CPT-1 expression increased after 10 weeks of ECH treatment, whilst CD36 levels decreased ($^{\#\#}$p<0.01), indicating that ECH activated cardiac PPAR-α/M-CPT-1 signaling in *db/db* mice.

Discussion

In 1972, Ruble identified small vessels in the myocardium[25] that occurred as a result of stenosis, thickening of the tube wall and diffuse fibrosis of the interstitium. The first concept of DCM was proposed when dissecting the hearts of diabetic patients. This excluded coronary artery sclerosis, and was later confirmed by Kannu and colleagues.

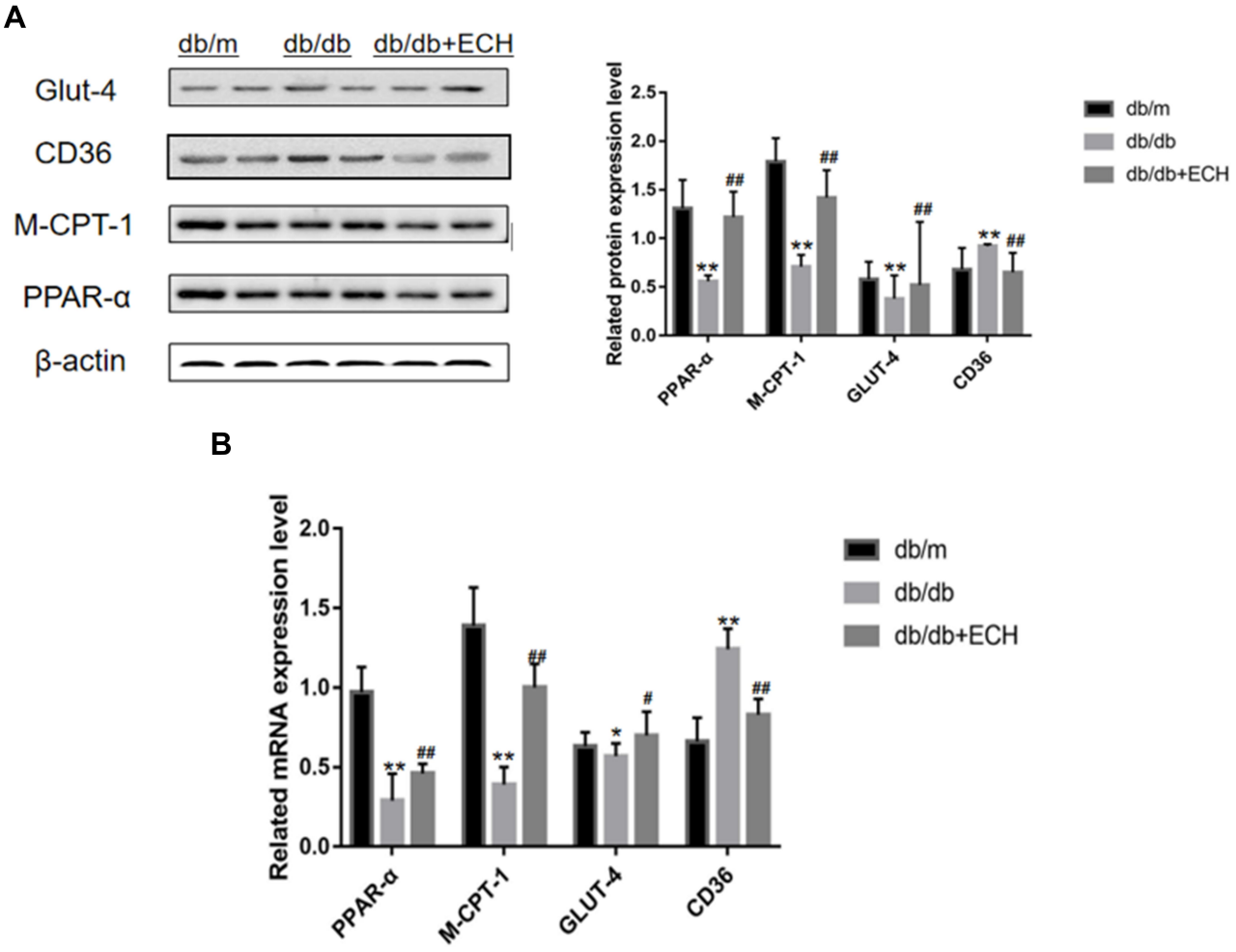

Figure 9 Western blot analysis of PPAR-α, M-CPT-1, CD36, GLUT-4 (**A**) and RT-PCR analysis of PPAR-α, M-CPT-1, CD36, GLUT-4 (**B**).
Notes: Data are expressed as mean±SD. db/m group n=9, all other groups n=10; *p < 0.05 or **p < 0.01 vs db/m group, $^{\#}$p < 0.05 or $^{\#\#}$p < 0.01 vs db/db group.
Abbreviations: ECH, echinacoside; PPAR-α, peroxisome proliferators-activated receptor-α; M-CPT-1, muscle-carnitine palmitoyl transferase-1; GLUT-4, glucose transporter-4.

Diabetic cardiomyopathy is generally divided into four stages. In the first stage, left ventricular mass increased, diastolic dysfunction and ejection fraction (EF) normal. Even clinically asymptomatic, myocardial fibrosis increased, early diastolic filling decreased, and left ventricular end-diastolic pressure increased.[22] The second stage is characterized by increased left ventricular mass, thickened ventricular walls, systolic and diastolic dysfunction (EF<50%), mild cardiac dilatation. In the third stage, diastolic dysfunction and arterial hypertension contribute to systolic dysfunction and microangiopathy. Stage IV, moderate-severe systolic dysfunction, cardiac dilatation, fibrosis, and microvascular and macrovascular lesions cause severe and irreversible changes in heart tissue ultimately.[26] Myocardial cell apoptosis, necrosis, hypertrophy, and fibrosis increase leading to disorders of diastolic and systolic functioning.[6,27] This eventually develops into ischemic heart disease and heart failure.[28] In this study, blood glucose and serum lipid levels of *db/db* mice significantly increased in the *db/db* group. Symptoms of obesity were also observed, including body weight changes and increases in the rate of HW/TL compared to the *db/m* group. HE staining and Masson's trichrome staining of the heart showed obvious pathological changes in the cardiac myocytes of the *db/db* group, including hypertrophy and necrosis, disordered cardiac myocytes, and high levels of extracellular matrix deposition. These data indicate that *db/db* mice exhibit early DCM under long-term hyperglycemia.

ATP is the basic energy source for the heart. Cardiac energy is provided by the oxidation and decomposition of FA, that accounts for ~70% of the cardiac energy supply.[29] The remainder is provided by carbohydrates such as glucose and lactic acid.[30] Diabetic hearts are subject to increased energy consumption and imbalances in myocardial capacity, representing the principal cause of myocardial metabolic disorders, including decreased glucose metabolism and increased FA metabolism. This leads to increased FA uptake and oxidation leading to adipose accumulation and the formation of toxic fat substances, directly leading to DCM lesions.[31]

PPAR-α is a member of the nuclear receptor superfamily and is distributed in the liver, kidney, skeletal muscle and heart tissues of animals.[12,15,32] PPAR-α regulates fat and glucose metabolism, inflammatory responses, cell cycle progression, and immune responses through gene transcription. Recent studies show that PPAR-α is closely related to cardiac metabolism and disease progression during DCM.[33,34] As a downstream gene regulated by PPAR-α, M-CPT-1 regulates the metabolism of long-chain fatty acids in cardiomyocytes to inhibit lipid toxicity.[9,11] In this study, we found that CD36 is overexpressed in the cardiomyocytes of *db/db* diabetic mice leading to increased FA uptake in cardiomyocytes. PPAR-α/M-CPT-1 levels were significantly lower than those of *db/db* mice, leading to the repressed clearance of lipid metabolites in cardiomyocytes, further aggravating lipid toxicity. Conversely, during DCM, PPAR-α inhibits glucose uptake through the down-regulation of GLUT-4. In the stage of disease compensation, in order to maintain the normal functionality of cardiomyocytes, the expression level of CD36 is compensatory overexpression and uptake of FA by cardiomyocytes was increased. Due to excessive FA uptake and oxidation, myocardial cells are in a continual state of oxidative stress, evidenced through the levels of antioxidant indicators including SOD, GSH-px and MDA. This was also reflected in Tunel assays and through assessments of the oxidation index and antioxidant levels.

The body weight of *db/db*+ECH mice was significantly lower than that of *db/db* mice. Although blood glucose levels were not reduced to levels comparable to the *db/m* group, ECH caused significant improvements in blood glucose levels compared to the *db/db* group. HE staining, Masson´s trichrome staining and Sudan II staining showed that, compared to the *db/db* group, cardiomyocyte morphology was alleviated following ECH intervention in *db/db* mice, with reduced intercellular spaces, improved extracellular matrix deposition, and lower levels of lipid accumulation.

ECH also improved lipid metabolism in *db/db* DCM. Accumulating biochemical evidence suggests that ECH improves serum lipid levels in DCM (Table 2). Through Western blot and RT-PCR analysis, ECH improved lipid accumulation in cardiomyocytes through the upregulation of PPAR-α expression, subsequently leading to the activation of M-CPT-1 and a loss of CD36 expression. This ultimately inhibited FA uptake in cardiomyocytes. GLUT-4 promotes glucose utilization in cardiomyocytes and stabilizes the balance between glucose and lipid metabolism. ECH up-regulates antioxidant genes and down-regulates pro-oxidation genes, improving oxidative stress injury in myocardial cells. We found that ECH also upregulates the PPAR-α/M-CPT-1 axis and down-regulates PPAR-α/GLUT-4 pathways to control lipid toxicity in DCM.

Conclusions

In *db/db* mice with diabetic myocardium, glucose and lipid metabolism are dysregulated, leading to increased levels of oxidative stress and apoptosis. This study confirmed that ECH can significantly reduce long-term hyperglycemia in *db/db* mice through PPAR/M-CPT-1/GLUT-4 signaling. Meanwhile, ECH improved oxidative stress and inhibited myocardial apoptosis in *db/db* DCM mice, which may be related to improved energy metabolism. Whilst the underlying mechanisms governing these effects were not discovered, these findings provide a new direction for the treatment of DCM and the protective role of ECH in improving myocardial injury.

Data Sharing Statement

All data generated or analyzed during this study are included in this published article.

Ethics Approval

All procedures involving animals were in accordance with the ethical standards of the experimental animal ethics committee of Renmin Hospital of Wuhan University affiliated to the animal feeding center of Renmin Hospital of Wuhan University, permit number (WDRM2010517).

Acknowledgments

The study was supported by the Hubei Natural Science Foundation of China Grant No.2016CFB673.

Author Contributions

All authors made substantial contributions to conception and design, acquisition of data, or analysis and interpretation of data; took part in drafting the article or revising it critically for important intellectual content; agreed to submit to the current journal; gave final approval of the version to be published; and agree to be accountable for all aspects of the work.

Disclosure

The authors declare that they have no conflicts of interest.

References

1. Bauters C, Lamblin N, Mc Fadden EP, Van Belle E, Millaire A, de Groote P. Influence of diabetes mellitus on heart failure risk and outcome. *Cardiovasc Diabetol*. 2003;1(8):1–2. doi:10.1186/1475-2840-2-1
2. Tate M, Grieve DJ, Ritchie RH. Are targeted therapies for diabetic cardiomyopathy on the horizon? *Clin Sci*. 2017;131(10):897–915. doi:10.1042/CS20160491
3. Khan H, Anker SD, Januzzi JJ, et al. Heart failure epidemiology in patients with diabetes mellitus without coronary heart disease. *J Card Fail*. 2019;25(2):78–86. doi:10.1016/j.cardfail.2018.10.015
4. Sheila K, Patel B. The CTGF gene −945 G/C polymorphism is not associated with cardiac or kidney complications in subjects with type 2 diabetes. *Cardiovasc Diabetol*. 2012;1(11):42.
5. Alonso N, Moliner P, Mauricio D. Pathogenesis, clinical features and treatment of diabetic cardiomyopathy. *Adv Exp Med Biol*. 2018;1067:197–217.
6. Jia G, Whaley-Connell A, Sowers JR. Diabetic cardiomyopathy: a hyperglycaemia- and insulin-resistance-induced heart disease. *Diabetologia*. 2018;61(1):21–28. doi:10.1007/s00125-017-4390-4
7. Bell D, Goncalves E. Heart failure in the patient with diabetes: epidemiology, aetiology, prognosis, therapy and the effect of glucose-lowering medications. *Diabetes Obes Metab*. 2019;6(21):1277–1290. doi:10.1111/dom.13652
8. Dong C, Zhou H, Shen C, et al. Role of peroxisome proliferator-activated receptors gene polymorphisms in type 2 diabetes and metabolic syndrome. *World J Diabetes*. 2015;6(4):654–661. doi:10.4239/wjd.v6.i4.654
9. Kallwitz ER, McLachlan A, Cotler SJ. Role of peroxisome proliferators-activated receptors in the pathogenesis and treatment of nonalcoholic fatty liver disease. *World J Gastroenterol*. 2008;14(1):22–28. doi:10.3748/wjg.14.22
10. Ip E, Geoffrey C, Farrell M, et al. Central role of PPARα-dependent hepatic lipid turnover in dietary steatohepatitis in mice. *Hepatology*. 2003;38(1):123–132. doi:10.1053/jhep.2003.50307
11. Watts GF, Barrett PHR, Ji J. Differential regulation of lipoprotein kinetics by atorvastatin and fenofibrate in subjects with the metabolic syndrome. *Diabetes*. 2003;52(3):803–811. doi:10.2337/diabetes.52.3.803
12. Li F, Patterson AD, Krausz KW, et al. Metabolomics reveals an essential role for peroxisome proliferator-activated receptor α in bile acid homeostasis. *J Lipid Res*. 2012;53(8):1625–1635. doi:10.1194/jlr.M027433
13. Fraulob FJ, Souza-Mello V, Aguila AM, et al. Beneficial effects of rosuvastatin on insulin resistance, adiposity, inflammatory markers and non-alcoholic fatty liver disease in mice fed on a high-fat diet. *Clin Sci*. 2012;123(4):259–270. doi:10.1042/CS20110373
14. Gore PN, Badar V, Hardas M, Bansode V. Comparative effect of telmisartan vs lisinopril on blood pressure in patients of metabolic syndrome. *Endocr Metab Immune Disord Drug Targets*. 2015;15(1):64–70. doi:10.2174/1871530314666141128154152
15. Everett L, Galli A, Crabb D. The role of hepatic peroxisome proliferator-activated receptors (PPARs) in health and disease. *Liver*. 2000;20(3):191–199. doi:10.1034/j.1600-0676.2000.020003191.x
16. Song S, Zhang L, Cao J, et al. Characterization of metabolic pathways and absorption of sea cucumber saponins, holothurin A and echinoside A, in vitro and in vivo. *J Food Sci*. 2017;82(8):1961–1967. doi:10.1111/1750-3841.13759
17. Wu Y, Li L, Wen T, et al. Protective effects of echinacoside on carbon tetrachloride-induced hepatotoxicity in rats. *Toxicology*. 2007;232(-1–2):50–56. doi:10.1016/j.tox.2006.12.013
18. Xiong WT, Gu L, Wang C, et al. Anti-hyperglycemic and hypolipidemic effects of Cistanche tubulosa in type 2 diabetic db/db mice. *J Ethnopharmacol*. 2013;150(3):935–945. doi:10.1016/j.jep.2013.09.027
19. Hiroshi Shimoda JT, Tanaka J, Takahara Y, Takemoto K, Shan S-J, Su M-H. The hypocholesterolemic effects of istanche tubulosa extract, a chinese traditional crude medicine, in mice. *Am J Chin Med*. 2009;37(06):1125–1138. doi:10.1142/S0192415X09007545
20. Tang F, Hao Y, Zhang X, et al. Effect of echinacoside on kidney fibrosis by inhibition of TGF-β1/Smads signaling pathway in the db/db mice model of diabetic nephropathy. *Drug Des Devel Ther*. 2017;11:2813–2826. doi:10.2147/DDDT.S143805

21. Xie H, Chung DY, Kura S, et al. Differential effects of anesthetics on resting state functional connectivity in the mouse. *J Cereb Blood Flow Metab*. 2020;40(4):875–884. doi:10.1177/0271678X19847123
22. EWestermeier F, ERiquelme J, EPavez M, et al. New molecular insights of insulin in diabetic cardiomyopathy. *Front Physiol*. 2016;7:125.
23. Qi L, Qin J, Li G, et al. Exploration of α-glucosidase inhibitor with anti-diabetic effects from novel bio-resources. Global Chinese Health (Functional) Food Technology Conference; 2013.
24. Kuroda T, Hirota H, Fujio Y. Carbacyclin induces carnitine palmitoyltransferase-1 in cardiomyocytes via peroxisome proliferator-activated receptor (PPAR) delta independent of the IP receptor signaling pathway. *J Mol Cell Cardiol*. 2007;43(1):54–62. doi:10.1016/j.yjmcc.2007.04.003
25. Rubler S, Dlugash J, Yuceoglu YZ, Kumral T, Branwood AW, Grishman A. New type of cardiomyopathy associated with diabetic glomerulosclerosis. *Am J Cardiol*. 1972;30(6):595–602. doi:10.1016/0002-9149(72)90595-4
26. Gilca GE, Stefanescu G, Badulescu O, Tanase D-M, Bararu I, Ciocoiu M. Diabetic cardiomyopathy: current approach and potential diagnostic and therapeutic targets. *J Diabetes Res*. 2017;5:1–7. doi:10.1155/2017/1310265
27. Sung MM, Hamza SM, Dyck JRB. Myocardial metabolism in diabetic cardiomyopathy: potential therapeutic targets. *Antioxid Redox Sign*. 2015;22(17):1606–1630. doi:10.1089/ars.2015.6305
28. Fillmore N, Mori J, Lopaschuk GD. Mitochondrial fatty acid oxidation alterations in heart failure, ischaemic heart disease and diabetic cardiomyopathy. *Br J Pharmacol*. 2014;171(8):2080–2090. doi:10.1111/bph.12475
29. Jansen MA, Shen H, Zhang L, et al. Energy requirements for the Na+ gradient in the oxygenated isolated heart: effect of changing the free energy of ATP hydrolysis. *Am J Physiol*. 2003;285(6):2437–2445.
30. Daifen H. Expression of genes participating in regulation of fatty acid and glucose utilization and energy metabolism in developing rat hearts. *Am J Physiol*. 2004;287(5):2035–2042.
31. van de Weijer Tineke B, Patrick S. Lipotoxicity in type 2 diabetic cardiomyopathy. *Cardiovasc Res*. 2011;92(1):54–62.
32. Shaherin B, Balachandran M, Hwan ST, et al. A molecular dynamics approach to explore the intramolecular signal transduction of PPAR-α. *Int J Mol Sci*. 2019;20(7).
33. Chen W, Xia Y, Zhao X, et al. The critical role of Astragalus polysaccharides for the improvement of PPARalpha correction of PPRAalpha-mediated lipotoxicity in diabetic cardiomyopathy. *PLoS One*. 2012;7(10):e45541. doi:10.1371/journal.pone.0045541
34. Wu L, Wang K, Wang W, et al. Glucagon-like peptide-1 ameliorates cardiac lipotoxicity in diabetic cardiomyopathy via the PPARα pathway. *Aging Cell*. 2018;17(4):e12763. doi:10.1111/acel.12763